Catalysis Today 139 (2008) 180–187

Contents lists available at ScienceDirect

Catalysis Today

journal homepage: www.elsevier.com/locate/cattod

Formation and structure of Au/TiO_2 and Au/CeO_2 nanostructures in mesoporous SBA-15

A. Beck [a], A. Horváth [a], Gy. Stefler [a], R. Katona [a], O. Geszti [b], Gy. Tolnai [c], L.F. Liotta [d], L. Guczi [a,*]

[a] Institute of Isotopes, HAS, P.O. Box 77, H-1525 Budapest, Hungary
[b] Research Institute for Technical Physics and Materials Science, HAS, Konkoly Thege Miklós út 29/33, H-1525 Budapest, Hungary
[c] Institute of Surface Chemistry and Catalysis, Chemical Research Center, HAS, P.O. Box 17, H-1025 Budapest, Hungary
[d] Istituto per lo Studio dei Materiali Nanostrutturati, CNR, Via Ugo La Malfa, 90146 Palermo, Italy

ARTICLE INFO

Article history:
Available online 19 August 2008

Keywords:
Au/SBA-15
TiO_2
CeO_2 decoration
Stabilization of Au nanoparticles
CO oxidation

ABSTRACT

The catalytic activity of gold nanoparticles deposited on the SBA-15 and modified by various oxide promoters has been investigated. 5 wt.% TiO_2 was introduced into SBA-15 (sample denoted by *TiSBA*). Gold using $HAuCl_4$ precursor was deposited (i) by deposition–precipitation (DP) (*AuTiSBA_DP*), (ii) by adsorption of Au colloid previously prepared by $NaBH_4$ reduction, and stabilized by polyvinylalcohol (PVA) (*AuTiSBA_PVA*) and (iii) by $NaBH_4$ reduction of Au precursor in the presence of poly(diallyldimethylammonium) chloride (PDDA) in the suspension of the support (*AuTiSBA_PDDA*). Au/5 wt.% TiO_2/SiO_2 reference sample (*AuTiSiO2_DP*) was prepared using high surface area amorphous silica by similar TiO_2 introduction and DP of Au. The Au/SBA-15 references (*AuSBA_PVA*, *AuSBA_PDDA*) were made by gold deposition type (ii) and (iii) on SBA-15. 5 wt.% TiO_2 and 10 wt.% CeO_2 containing SBA-15 supported gold were prepared via impregnation of *AuSBA_PVA* by Ti(IV) bis(ammoniumlactato)dihydroxide (TALH) and $Ce(NO_3)_3$ solutions (*AuSBA_PVA_Ti*, *AuSBA_PVA_Ce*), respectively. All the samples were calcined before catalytic measurements and were characterized by BET technique, transmission electron microscopy (TEM) with EDS and X-ray diffraction (XRD). The activity sequence in the CO oxidation was *AuSBA_PVA_Ce* > *AuTiSBA_DP* > *AuTiSBA_PVA* > *AuSBA_PVA_Ti* ≈ *AuSBA_PVA* > *AuTiSiO2_DP* > *AuTiSBA_PDDA* > *AuSBA_PDDA*. The activity is strongly affected by gold/oxide interface (the length of Au-TiO_2 and Au-CeO_2 perimeter), which emerged during the preparation and discussed in terms of the surface charges of the components. The Au nanoparticles in the SBA-15 could be stabilized more efficiently than those on amorphous silica.

1. Introduction

It is generally accepted that SiO_2 is classified as non-active support regardless of whether the gold containing samples prepared by wet chemical technique [1–3] or by using model SiO_2/Si(1 0 0) system [4,5]. There have been several attempts to fabricate active Au on silica samples, but only the use of a gold cationic complex precursor $[Au(en)_2]^{3+}$ (ethylenediamine) via a wet chemical process proved to be successful [6,7]. Nevertheless, amorphous silica was also employed by the same research group to stabilize gold particle size deposited on TiO_2 support [8].

Stabilization of small gold nanoparticles looked feasible when a zeolite framework had been used to host small metal or bimetallic particles. Recently Somorjai et al. [9,10] synthesized mesoporous silica SBA-15 around metal nanoparticles in the 2–10 nm range. They found that the mesoporous channels expanded in order to accommodate the metal particles. Other efficient method has also been developed to synthesize highly active Au catalysts supported on mesoporous silica SBA-15 [7]. Gold cationic precursor was immobilized on negatively charged surfaces of silica by a unique DP method that makes use of the deprotonation reaction of ethylenediamine ligands. The resulting mesoporous catalyst was highly active for CO oxidation at or below room temperature. The pH value of the gold precursor solution dictated the catalytic activity through deprotonation of $[Au(en)_2]^{3+}$ ions and the surface interaction of silica with the gold precursor. Au nanoparticles inside mesopores became a stable catalyst.

* Corresponding author.
E-mail address: guczi@sunserv.kfki.hu (L. Guczi).

0920-5861/$ – see front matter © 2008 Elsevier B.V. All rights reserved.
doi:10.1016/j.cattod.2008.05.039

In another technique SBA-15 was functionalized by organosilane to generate a monolayer of positively charged groups on the pore surface to facilitate uniform distribution of ion-exchanged $[AuCl_4]^-$-metal precursors in the channel of SBA-15 [11]. This allowed under mild condition metal incorporation at higher metal loading and after reduction with $NaBH_4$ spherical Au particles were formed inside the channels. The rate of CO oxidation was found for this composite material much higher than any other Au/SiO_2 system. Similar method was utilized to prepare Pd nanoparticles in micropores. This method provided a general route for creating local environments within nanometer size pore structure [12].

One of the developments was to modify the SBA-15 support. On acidic Al-SBA-15 support uniformly distributed gold nanoparticles with sizes 2.7 nm were obtained by a successive procedure of aminosilane grafting and gold adsorption-reduction [7,13,14]. The catalyst, after activation by a high-temperature hydrogen treatment exhibited enhanced activity for CO oxidation at low temperature and the activity was dependent on the Si/Al ratio of the support. Oxygen adsorption on the defect sites of aluminosilicate produced by high-temperature hydrogen reduction created superoxide species facilitating the CO oxidation.

Highly dispersed gold nanoparticles were synthesized within the channels of a mesoporous SBA-15 support modified by TiO_2. The catalytic performance of the Au/Ti-SBA-15 materials was evaluated in the direct epoxidation of propene using a mixture of H_2 and O_2. The reaction data indicated that Au/Ti-SBA-15 materials obtained by Ti grafting have higher catalytic activity than the samples in which Ti-SBA-15 was obtained by direct synthesis [15]. These differences in catalytic behaviour were attributed to the differences in the amount and dispersion of Ti within the mesoporous silica support, as well as to differences in the Au nanoparticle size.

Similar techniques have demonstrated the beneficial effect of modification of SBA-15 sample [16–21]. TiO_2 monolayer grafted improved the gold activity in the CO oxidation. Gold nanoparticles (0.8–1 nm) were deposited on titania-modified SBA-15 via a deposition–precipitation method and X-ray diffraction (XRD) pattern showed that gold existed as Au^{3+} and Au^0 in the as-synthesized and reduced catalyst, respectively [16]. Other oxides such as cobalt-oxide exerted similar effect. Cobalt-containing SBA-15 supported gold catalysts for low-temperature CO oxidation were prepared [22]. It was shown that Co_3O_4 stabilizes the highly dispersed gold deposited on SBA-15 and the strong metal-support interaction between gold and cobalt oxides increased the activity in the CO oxidation.

Similar functionalization technique described above has been successfully applied to fabricate active oxide layer decorating either the surface of amorphous silica, or the deposited gold surface [23–25]. It was clearly indicated that amorphous TiO_2 prepared by wet chemical technique increased the CO oxidation activity of the gold sol deposited as nanoparticles on inert support. The successful functionalization that was observed for gold sol derived Au on amorphous silica support can be induced for mesoporous SBA-15 and it can be modified similarly to that observed for both TiO_2 and cobalt oxide.

In the present work we aim at fabricating the similar Au-TiO_2 and Au-CeO_2 nanostructures in a mesoporous SBA-15 to mimic 3D nano-system. Different preparation procedures will be employed and compared to reach stable, well dispersed system with large Au-TiO_2 and Au-CeO_2 interface and perimeter. In the preparation gold sol will be predominantly used for Au introduction and different precursors for addition of active oxide, the order of the deposition of gold and oxide will be varied, as well. The samples will be characterized by XRD, TEM, HRTEM, zeta potential measurements and the CO oxidation will be used as test reaction.

2. Experimental

2.1. Sample preparation

For preparation of *SBA-15* 2.0 g P123 block copolymer, 45 g water and 30 mg 4 M HCl was mixed, then 3.1 g tetra-ethyl-orthosilicate (TEOS) was added and was stirred at 40 °C for 20 h. The gel formed was hydrothermally treated in an autoclave at 100 °C for 24 h, then filtered and dried at room temperature. The template was removed by calcination at 450 °C in oxygen for 5 h preceded by heating up by 2 °C/min rate in nitrogen. 5 wt.% TiO_2 was introduced by surface hydroxyl initialized hydrolysis of Ti-isopropoxide in anhydrous ethanol suspension of SBA-15 under reflux followed by evaporation of liquid, drying and calcination in air at 400 °C for 4 h (sample denoted by *TiSBA*). 2 wt.% of gold was intended to deposit on three different ways using $HAuCl_4$ precursor (i) by deposition–precipitation (DP) using Na_2CO_3 (*AuTiSBA_DP*), (ii) by preparation of Au colloid (*Au_PVA*) reducing $HAuCl_4$ (0.48 mM) at room temperature with $NaBH_4$ (2.42 mM) in presence of polyvinylalcohol (PVA) (64 mg/l) as stabilizer [26] followed by adsorption of *Au_PVA* on SBA-15 at pH 1.5 (*AuTiSBA_PVA*) and (iii) by reduction of Au precursor (0.45 mM) with $NaBH_4$ (2.23 mM) in presence of poly(diallyldimethylammonium) chloride (PDDA) (86 mg/l) in the aqueous suspension of the support (*AuTiSBA_PDDA*). All the preparation systems were filtered, washed thoroughly and dried at 60–80 °C. Au/5 wt.% TiO_2/SiO_2 reference sample (*AuTiSiO$_2$_DP*) was prepared using high surface area (478 m^2/g, 6.6 nm pore mean diameter) amorphous silica by similar TiO_2 introduction and DP of Au. Au/SBA-15 references (*AuSBA_PVA*, *AuSBA_PDDA*) were made by gold deposition type (ii) and (iii) on SBA-15. 5 wt.% TiO_2 and 10 wt.% CeO_2 (same molar concentration for TiO_2 and CeO_2) containing SBA supported gold (*AuSBA_PVA_Ti*, *AuSBA_PVA_Ce*) were prepared by impregnation of *AuSBA_PVA* by aqueous solution of Ti(IV) bis(ammoniumlactato)dihydroxide (TALH) and $Ce(NO_3)_3$, respectively, with stirring at 40–50 °C for 40 min under reflux followed by evaporation of water at about 60–70 °C. *TiO$_2$* and *CeO$_2$* formed during calcination pretreatment applied before catalytic reactions. Pure TiO_2, CeO_2 and amorphous SiO_2 supported Au (*AuTiO$_2$_PVA* and *AuCeO$_2$_PVA* and *AuSiO$_2$_PVA*) were prepared by adsorption of *Au_PVA* sol at its original pH (pH 5–6) on Degussa P25 TiO_2 and Aldrich CeO_2 nanopowder and at pH 1.5 on Davisil SiO_2 followed by filtering, thorough washing and drying.

2.2. Sample characterization

The surface of the samples was measured by BET technique. The Ti and Au content of the samples were determined by a double-focusing inductively coupled plasma mass spectrometer (ICP-MS, ELEMENT2). All measurements were made using a Scott-type spray chamber operating at room temperature and a Meinhard concentric nebulizer. The catalyst samples were dissolved in HNO_3, HCl and HF acid mixture. Prior to the ICP-MS analysis the excess HF was removed. Au and Ti standards were used as reference.

The distribution and size of gold particles and TiO_2 and CeO_2 on SBA-15 was studied by a Philips CM20 transmission electron microscope (TEM) operating at 200 kV equipped with energy dispersive spectrometer (EDS) for electron probe microanalysis. The aqueous suspensions of the samples were dropped on carbon-coated grid and after evaporating water the electron micrographs of the particles were taken. The gold particle size distribution was obtained by measuring the diameter of about 200–300 metal particles. The *AuSBA_PVA_Ce* was investigated also in a JEOL 3010 high resolution transmission electron microscope (HRTEM) at 300 kV accelerating voltage with resolving power of 0.17 nm.

Table 1
Several characteristics of the samples

Samples	Preparation	Au (wt.%)	Surf. area (m^2/g)/pore diameter (nm)	d_{Au} (TEM) as prep. (nm)	d_{Au} (TEM) after cat. test (nm)	d_{Au} (XRD) after cat. test (nm)	d_{oxide} (XRD) after cat. test (nm)
References							
SBA	SBA-15	–	609/5.7	–	–	–	–
SBA_calc	*SBA* + 300 °C calc./16 h	–	580/5.7	–	–	–	–
TiSBA	(*SBA_calc* + Ti-isopropoxide) + calc.	–	556/5.6	–	–	–	–
Sol							
Au_PVA	($HAuCl_4$ + PVA) + $NaBH_4$	–	–	2.7 ± 0.9	–	–	–
Samples							
AuTiSBA_DP	*TiSBA* + $HAuCl_4$_DP	0.62		5.1 ± 2. 9	4.8 ± 1.8		
AuTiSiO$_2$_DP	(SiO_2 + Ti-isopropoxide) + calc. + $HAuCl_4$_DP	1.5		2.1 ± 0.5	16 ± 3.4		
AuSBA_PVA	*SBA* + *Au_PVA* (pH 1.5)	1.76		2.7[a]	4.0 ± 1.2		–
AuTiSBA_PVA	*TiSBA* + *Au_PVA* (pH 1.5)	2.47		2.7[a]	2.9 ± 1.0	3.6	<1 (TiO_2)
AuSBA_PVA_Ti	*AuSBA_PVA* + TALH_imp.	1.76		2.7[a]	n.a.	5.8	2.2 (TiO_2)
AuSBA_PVA_Ce	*AuSBA_PVA* + $Ce(NO_3)_3$_imp.	1.76		2.7	5.0 ± 1.8	5.2	4.8 (CeO_2)
AuSBA_PDDA	(*SBA* + PDDA + $HAuCl_4$) + $NaBH_4$	1.24		5.3 ± 2.4	5.5 ± 2.4		–
AuTiSBA_PDDA	(*TiSBA* + PDDA + $HAuCl_4$) + $NaBH_4$	1.47		5.7 ± 2.1	6.7 ± 3.6		
AuSiO$_2$_PVA	SiO_2 + *Au_PVA* (pH 1.5)	1.7	300/15.5	2.7[a]	7.9 ± 2.8		–
AuTiO$_2$_PVA	TiO_2 + *Au_PVA*	2.3	55/non-porous	2.7[a]	5.3 ± 2.1		34 (anatase) 52 (rutile)
AuCeO$_2$_PVA	CeO_2 + *Au_PVA*	2.2	80–100/non-porous	2.7[a]	5.6 ± 3.5	7.5	23 (CeO_2)

[a] Deduced from the particle size of the Au sol applied for the preparation.

X-ray diffraction measurements were carried out with a Philips Xpert powder diffractometer using Cu Kα radiation (λ = 0.15418 nm). The crystallite size of the different phases were calculated from the line broadening of the most intense reflections using the Scherrer equation [27,28].

Zeta potential of the different components of the catalyst preparation was determined by dynamic light scattering measurements using a Malvern Zeta Sizer (Nano Series NanoZS) apparatus to characterize the electrostatic interactions that may control the formation of the 3 component (Au, TiO_2 or CeO_2, SiO_2) composite system.

The CO oxidation was measured in a plug flow reactor at atmospheric pressure connected to a QMS type Balzers 100. Different amounts of catalyst containing the same amount of gold (1.4, 1.0 or 0.35 mg Au) were employed which were in situ calcined at 400 °C in 20% O_2 in He mixture for 1 h (10 °C/min heating rate, 30 ml/min gas flow) for the removal of organic residues. Temperature programmed reaction was performed with a 55 ml/min gas flow of 0.54% CO and 9.1% O_2 in He with 4 °C/min ramp rate. The conversion was calculated on the basis of the CO_2 production.

3. Results and discussion

In Table 1 the experimental data concerning the characterization of the various samples are presented. The gold content of the samples varies between 2.5 and 0.6 wt.% because the gold adsorption was different in the various preparation systems and some amount of Au was incidentally removed during the washing of the samples. The original surface area of SBA-15 (610 m^2/g) decreased by about 5% both after calcination and after introduction of TiO_2 giving 556 m^2/g surface area. The pore size did not change significantly being about 5.6–5.7 nm. The particle size of gold was determined by TEM measurements.

3.1. TEM measurements

Figs. 1–3 show the transmission electron micrographs of *TiSBA*, *AuTiSBA_DP* and *AuTiSBA_PVA* samples after calcination and catalytic test. The channels are giving a regular spacing. Titania cannot be distinguished on the images, but according to EDS measured on different spots it was well distributed on the samples.

The gold nanoparticles are evenly distributed on the SBA-15 support and can be located inside the channels even after the CO oxidation. In the *AuTiSBA_DP*, *AuTiSBA_PDDA* and *AuSBA_PDDA* samples the gold nanoparticles prepared from $AuCl_4^-$ precursors can be formed inside the channels if these ions migrate into the pore system before hydrolysing or reducing. Regarding the sol derived samples the mean diameter of the preformed particles of *Au_PVA* sol is about half of the mean pore diameter of the support according to TEM measurements. The polymer shell stabilizing the Au nanoparticles cannot be seen by TEM, therefore, the hydrodynamical size of the Au particles was checked by dynamic light scattering measurements. The hydrodynamical size (3.8 ± 0.8 nm)

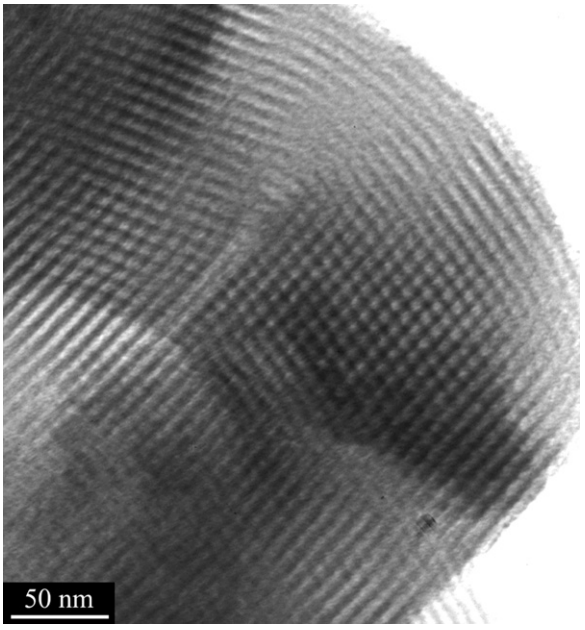

Fig. 1. TEM image of *TiSBA*.

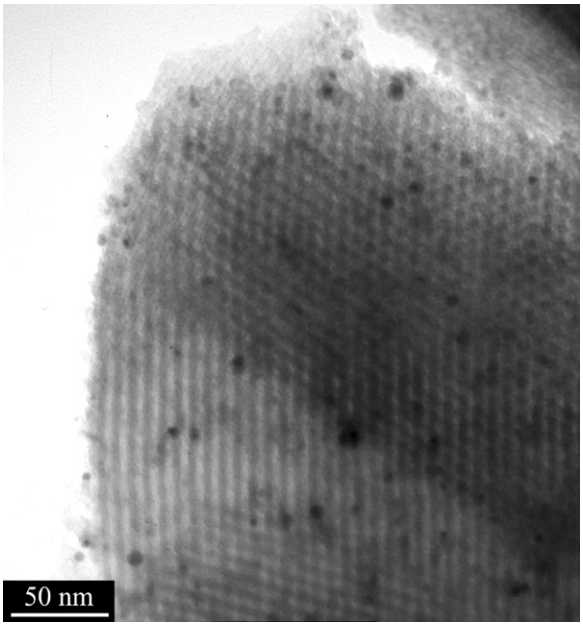

Fig. 2. TEM image of *AuTiSBA_DP* after catalytic test.

is about 1 nm larger than the Au size determined by TEM (d_{Au} = 2.7 ± 0.9 nm). This is still significantly smaller than the pore diameter, thus the Au particles stabilized by PVA (*Au_PVA)* can also diffuse into the channels.

The original gold particles derived from *Au_PVA* sol (2.7 ± 0.9 nm) were monodisperse in the samples and smaller than those in situ formed and located in the SBA-15 support (*AuTiSBA_DP* (5.1 ± 2.9 nm), *AuSBA_PDDA* (5.3 ± 2.4 nm), *AuTiSBA_PDDA* (5.7 ± 2.1 nm). In the latter samples the mean diameter of gold is about the same as the mean pore diameter of the mesoporous support suggesting the existence of some limitation of the particle growth. The stability of the gold sizes during the calcination pretreatment and the catalytic reaction supports this assumption. In the sol derived *AuSBA_PVA* and its derivative *AuSBA_PVA_Ce* the sintering of gold nanoparticles during calcination and reaction resulted in 4.0 ± 1.2 and 5.0 ± 1.8 nm mean diameter, respectively. In the TiO_2 containing *AuTiSBA_PVA* samples the sintering were retarded and the size of gold particles after calcination and reaction is hardly larger (2.9 ± 1.0 nm) than the original value. On the contrary, in the amorphous silica supported *AuTiSiO$_2$_DP* the Au mean diameter in the as prepared state (2.1 ± 0.5 nm) increased tremendously (16 ± 3.4 nm) under the thermal treatments, which suggest that the Au nanoparticles are stabilized by the SBA-15 structure, consequently they must be present mostly in the mesopores.

Finally, we compared the size of gold samples on pure SiO_2, TiO_2 and CeO_2 supports. The size increased slightly on TiO_2 and CeO_2 during the catalytic test and preceded calcination (d_{Au} = 5.3 ± 2.1 and 5.6 ± 3.5 nm, respectively), while on amorphous SiO_2 the sintering was more significant, providing d_{Au} = 7.9 ± 2.8 nm, much larger particles than in the analogous SBA-15 supported *AuSBA_PVA* (4.0 ± 1.2 nm).

HRTEM images were taken on the most active *AuSBA_PVA_Ce* sample after catalytic test (see Fig. 4). Crystalline CeO_2 patches of several nm lateral dimensions can be seen mostly in the vicinity of Au particles.

3.2. XRD measurements

The *Au_PVA* sol derived TiO_2 and CeO_2 containing SBA-15 supported samples, *AuTiSBA_PVA*, *AuSBA_PVA_Ti*, *AuSBA_PVA_Ce* and the reference *AuTiO$_2$_PVA* and *AuCeO$_2$_PVA* were measured by XRD after catalytic test to estimate the size of the crystalline phases (see Table 1 and Fig. 5). The Au particle sizes determined by TEM and XRD agree relatively well except in case of CeO_2 supported sample. The differentiation between gold and CeO_2 particles is a bit difficult on the TEM images that can be the reason the lower size estimated from TEM. Regarding the active oxide component of the samples, their crystallite sizes are significantly smaller (hardly detectable and about 2 nm for TiO_2 in *AuTiSBA_PVA* and *AuSBA_PVA_Ti*, respectively, and about 5 nm for CeO_2 in *AuSBA_PVA_Ce*) as they are applied as promoters than in the commercial nanopowders (34 and 52 nm for anatase and rutile in Degussa P25 TiO_2; 23 nm for CeO_2) used as support.

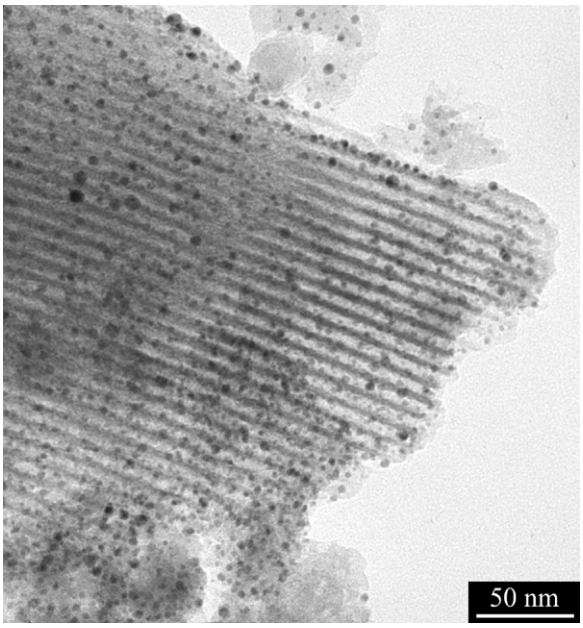

Fig. 3. TEM image of *AuTiSBA_PVA* after catalytic test.

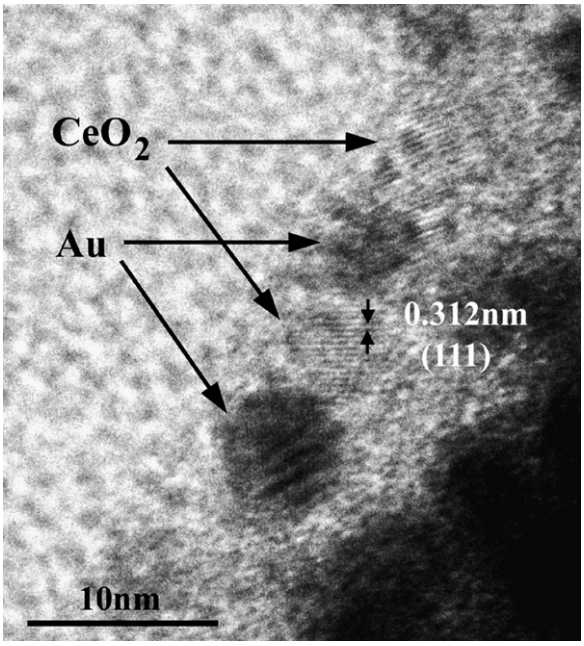

Fig. 4. HRTEM image of *AuTiSBA_PVA_Ce* after catalytic test.

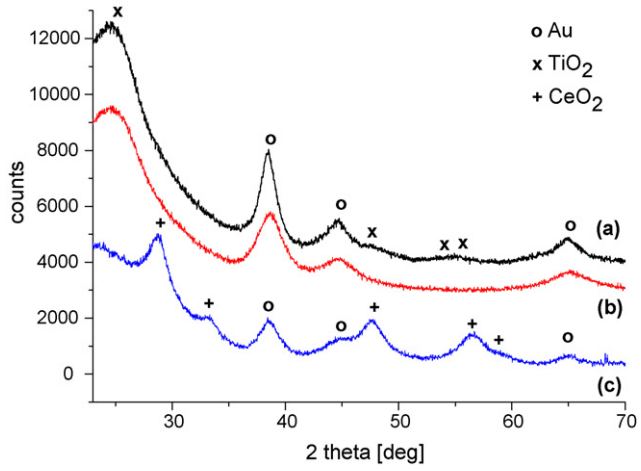

Fig. 5. XRD of *AuSBA_PVA_Ti* (a), *AuTiSBA_PVA* (b), *AuSBA_PVA_Ce* (c) samples after catalytic test.

3.3. Zeta potential measurements

In order to develop interface as large as possible between Au nanoparticles and the active oxide component (TiO_2 or CeO_2) on SBA-15 surface we have to control the attraction between them. Preparation of the sol based catalyst samples by adsorption of the sol on the support surface is dictated by the surface electric charging of the components as earlier we have detailed [24]. Accordingly, when gold sol is prepared from $HAuCl_4$ by citrate/tannic acid reduction, the gold nanoparticles are expected to be negatively charged, therefore adsorption of the metal particles does not occur on SiO_2 due to charge repulsion between stabilized metal particles and silica surface charged negatively above pH 2–3. This is why poly(diallyldimethylammonium) chloride as polycation has been used to recharge the silica surface to be positive and helping thereby the adsorption of gold nanoparticles.

The same holds on SBA-15 and TiO_2/SBA-15 support and this is why we determined the zeta potential. In Fig. 6 the "titration" curve is presented for the change of the zeta potential of *TiSBA* vs. the amount of charging agent PDDA. Adding about 21–22 μl of 0.8 g/l PDDA solution to the 1 mg/1 cm^3 aqueous *TiSBA* suspension the originally negatively charged surface neutralised, and further

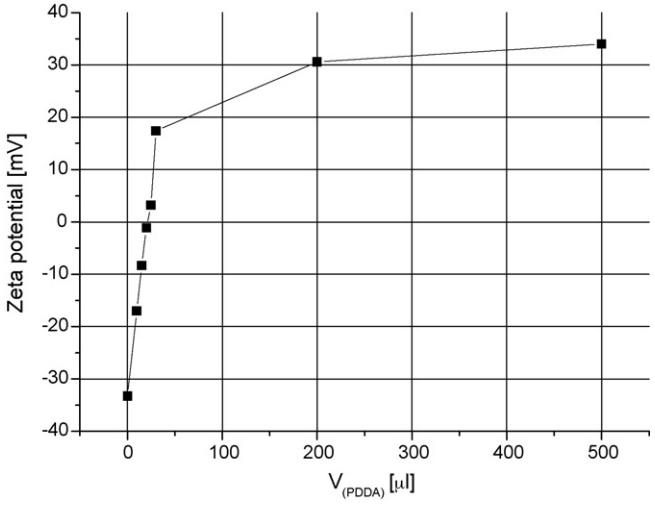

Fig. 6. Zeta potential of TiSBA-15 as a function of the amount of added 0.08 mg/cm^3 PDDA solution to the 10 cm^3 of 1 mg/cm^3 TiSBA-15 suspension.

Table 2
The average zeta potential for the various samples

Sample	Zeta potential	
	Average value (mV)	FWHM
SBA-15	−14.4	4.8
SBA-15, pH 2	0.5	18.1
TiSBA-15	−38.1	4.8
TiSBA-15, pH 2	6.9	16.1
Au_PVA	−45.4	26.9
AuSBA_PVA	−27.2	9.2

addition of PDDA increased the positive surface charge of the TiSBA-15 particles up to as high positive potential as negative was without PDDA addition. In the preparation of *AuSBA_PDDA* and *AuTiSBA_PDDA* 22 μl 0.8 g/l PDDA solution was given to 1 mg support in a more concentrated, 5.4 mg/cm^3 SBA-15 and TiSBA suspension, which appears sufficient to neutralize or charge the support slightly positive, thus, to eliminate the repulsion between the support surface and $[AuCl_4]^-$ ions, but it is not sufficient to create maximum attraction.

As shown in Table 2 both the surfaces of SBA-15 particles in the aqueous suspension and the Au nanoparticles in the sol stabilized by PVA, are negatively charged that explains why Au particles do not adsorb either on SBA-15 or TiO_2/SBA-15. The surface charge of the oxide support and the Au particles is originated predominantly from the protonation/deprotonation of the surface hydroxyl groups and of the alcoholic –OH groups of stabilizing PVA, respectively. Decreasing the pH of the aqueous SBA suspension to pH 2, the average zeta potential increases, it switches for positive value. The distribution of zeta potential becomes wider than it measured in the neutral suspension, thus, large amount of particles has positive surface charge attracting already the Au particles negatively charged even at this pH.

Since the TiO_2-modified SBA-15 in aqueous suspension shows a negative potential higher than SBA-15 itself, it seems that the charge density is higher after the TiO_2 deposition (hydroxyl concentration is higher on TiO_2, than on SBA-15). The average zeta potential for the *TiSBA* at pH 2 is positive and larger than in the case of SBA-15. It means that the TiO_2 patches must be more positive, so a preferable adsorption of Au nanoparticles with the negatively charged stabilizing shell on the titania surface can be expected. However, as the distribution of zeta potential is really wide both for Au sol and the supports at pH 2, this type of controlling effect is being weakened.

Because the surface charge of *AuSBA_PVA* in aqueous suspension is more negative than it is for SBA-15 itself it suggests that the surface of Au particles is more negative, than the surrounding support surface. During the impregnation of Au/SBA-15 with TALH or $Ce(NO_3)_3$ *AuSBA_PVA_Ti* and *AuSBA_PVA_Ce*, respectively, are produced. The deposition of negative Ti-precursor ion formed from TALH is likely favoured on the less negative, pure SBA-15 surface, while the positive Ce^{3+} ions are attracted rather by the Au surface, providing finally larger Au/CeO_2 than Au/TiO_2 interface and possibly also perimeter.

3.4. CO oxidation

Catalytic activities of the various samples related to the same Au content are compared on the basis of the CO conversion curves measured in the CO oxidation under standard conditions. The SBA-15 supported samples derived from *Au_PVA* sol and modified by TiO_2, CeO_2, can be compared in Fig. 7. After catalytic test the size of Au particles varies in the range of 2.9 and 5.0 nm. The *AuTiSBA_PVA* sample with the smallest Au size is more active than both

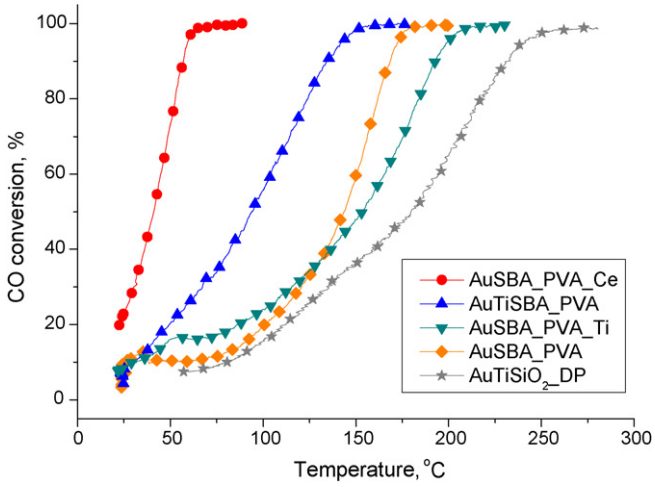

Fig. 7. CO oxidation conversion curves of *AuSBA_PVA_Ce*, *AuTiSBA_PVA*, *AuSBA_PVA_Ti*, *AuSBA_PVA* and *AuTiSiO$_2$_DP* (the Au loading in the catalytic reactor was 1.0 mg).

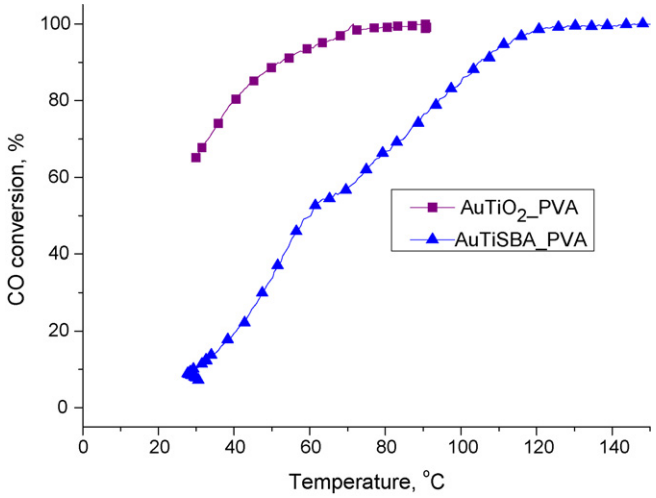

Fig. 9. CO oxidation conversion curves of *AuTiO$_2$_PVA* and *AuTiSBA_PVA* (the Au loading in the catalytic reactor was 1.4 mg).

AuSBA_PVA and *AuSBA_PVA_Ti*. It seems, that the activity of *AuSBA_PVA* is not improved by the post-deposition of titania using TALH. This finding can be interpreted by the zeta potential measurements, i.e. if there is a chance for the negatively charged Ti(IV)-bislactato-dihydroxid species resulting from TALH to be anchored either on SBA-15, or on Au nanoparticles, the bonding is preferred towards the less negative SBA-15 surface. This is supported by the comparison of the *AuSBA_PVA_Ti* and *AuTiSBA_PVA* samples. If SBA-15 is modified first with TiO_2, the SBA-15 and titania sites are competing for stabilized gold particles and as a result the negatively charged gold particles are attracted more strongly to the more positive titania. Thus, in the *AuTiSBA_PVA* sample the formation of longer perimeter of Au/titania interface is assumed to provide higher catalytic activity than that in the *AuSBA_PVA_Ti* sample. It has to be noted that the crystallite size of TiO_2 is really small, 2.2 nm in *AuSBA_PVA_Ti* and smaller than 1 nm in *AuTiSBA_PVA*. Especially the latter one, but both samples contain TiO_2 mostly in amorphous form.

Although in *AuSBA_PVA_Ce* sample the Au size is the largest and the CeO_2 crystallite size (4.8 nm) is also larger than that of TiO_2 in the titania containing systems, it is still the most active catalyst in the CO oxidation. We have to compare the *AuSBA_PVA_Ce* and the most active TiO_2 containing *AuTiSBA_PVA* sample. The sample promoted by ceria has obviously higher activity than that modified by titania which may be a consequence of the possibly longer Au/active oxide perimeter in case of *AuSBA_PVA_Ce*. This can likely be interpreted by the attraction between the Ce^{3+} ions and the negatively charged Au particles and SBA-15, and in this competition the Ce^{3+} ions prefer the interaction with gold possessing higher negative potential. However, there is no technique to quantitatively determine and to compare the Au/TiO_2 and Au/CeO_2 perimeters. Conversely, the catalytic activity could be estimation for the length of active perimeter if other factors affecting strongly the activity, as Au particle size, oxidation state of Au and the quality of the oxide can be regarded identical. Comparing titania and ceria, the presence of more mobile oxygen bonded to CeO_2 [29,30] shown e.g. in CO_2 reforming of methane on nanocrystalline $Ce_{0.8}Zr_{0.2}O_2$ support and finely dispersed nano size NiO_x crystallites and an abundance of mobile oxygen species in itself, may cause higher activity of Au/CeO_2 perimeter.

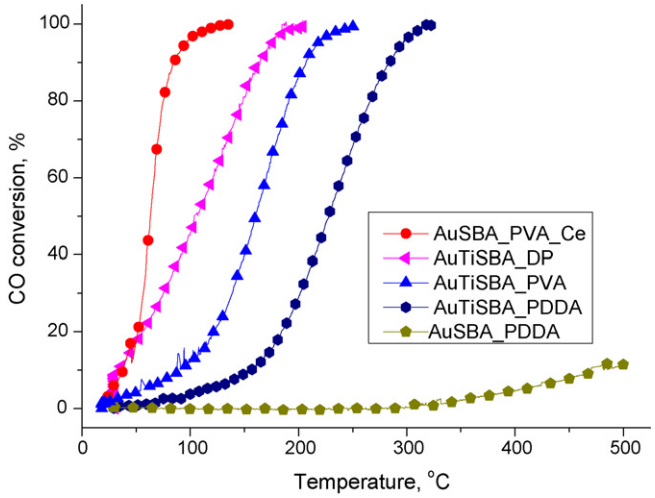

Fig. 8. CO oxidation conversion curves of *AuSBA_PVA_Ce*, *AuTISBA_DP*, *AuTiSBA_PVA*, *AuTiSBA_PDDA* and *AuSBA_PDDA* (the Au loading in the catalytic reactor was 0.35 mg).

In Fig. 8 the effect of various gold deposition techniques are compared. The *AuSBA_PDDA* sample is the least active, while when the SBA-15 has been modified first with Ti-isopropoxide the activity of the samples increases in a sequence of PDDA < PVA < DP. The Au particle size in the *AuTiSBA_PDDA* sample is the largest that can be one of the reasons for the lower activity. On the other hand, the final mean Au diameter is larger than the *TiSBA* pore size, consequently significant amount of Au should be on the outer surface of the support and some pores can be blocked by large particles. Note, the concentration of PDDA used to anchor the gold precursor to TiSBA-15 surface was not optimum, i.e. not enough to fully recharge the surface, so the reduction of $AuCl_4^-$ occurred rather in the liquid phase than on the surface.

Effect of the mesoporous structure in SBA-15 can be seen when *AuTiSBA_DP* and the amorphous silica supported *AuTiSiO$_2$_DP* (see Fig. 7 curve 5 and Fig. 8 curve 2) are compared. The higher catalytic activity of *AuTiSBA_DP* is probably due to the mesoporous structure confining the gold nanoparticles in the pores and thus being the growth of gold hampered unlike on the SiO_2 on which the mean diameter of gold (16 ± 3.4 nm) observed is a consequence of strong sintering during calcination.

In Figs. 9 and 10 the sol derived and TiO_2 promoted *AuTiSBA_PVA* as well as the CeO_2 promoted *AuSBA_PVA_Ce* samples are compared with *AuTiO$_2$_PVA* and *AuCeO$_2$_PVA* samples, sup-

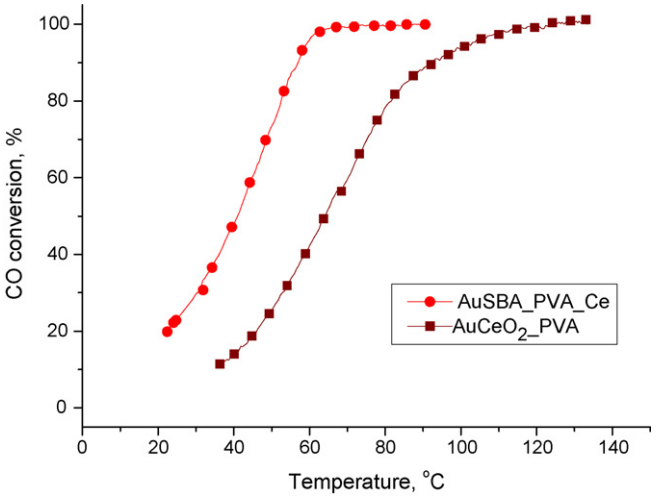

Fig. 10. CO oxidation conversion curves of *AuSBA_PVA_Ce* and *AuCeO$_2$_PVA* (the Au loading in the catalytic reactor was 1.0 mg).

ported on TiO_2 (Degussa P25) and CeO_2 nanopowder (Aldrich), respectively. Seemingly there is a contradiction between the two samples, namely, the activity of *AuTiO$_2$_PVA* is higher than that of *AuTiSBA_PVA*, whereas it is reverse for ceria the promoted sample, i.e. *AuSBA_PVA_Ce* is more active than *AuCeO$_2$_PVA*.

In the interpretation of the catalytic results two aspects should be addressed. The key issue is the gold particle size and equally important factor is the size of perimeter which is related to the gold/active oxide interface and the size of active oxide. Primarily the catalytic activity is controlled by the gold particle size. The gold particle size after the catalytic reaction is about the same (5.0–7.5 nm) in the *AuSBA_PVA_Ce* and the titania and ceria supported gold, while it is significantly smaller (2.9 nm) in *AuTiSBA_PVA* sample. The second factor is the interaction of gold nanoparticles with the titania or ceria promoter on the SBA-15 support. However, in this context we have to address the problem to two other factors, i.e. the surface charging during preparation controlling the interface formation and the size and morphology of oxide possibly affecting the activity of perimeter.

The term of perimeter was introduced by Haruta and co-workers [1,31–33]. In the Au/ZnO system the authors suggested that CO adsorbed at the perimeter interface and react with surface oxygen [31]. They also assumed that perimeter area of gold nanoparticles increased with a decrease of particles size for e.g. CO_2 adsorption in methanol synthesis [32] whereas in propylene epoxidation the oxygen was suggested to be adsorbed at the perimeter sites [33]. For Al_2O_3, SiO_2 and TiO_2 supported gold they also found the interface around gold particles essential for creation of the active sites in CO and hydrogen oxidation [1,34].

In preferential CO oxidation (PROX), in methane oxidation and in water gas shift reaction (WGS) the three way boundary has been emphasized [35–37]. Addition of MnO_x and FeO_x to Au/MgO/Al_2O_3 further enhanced the low-temperature CO oxidation with improved CO_2 selectivity. The increase in CO oxidation activity is attributed to supplying active oxygen via lattice oxygen. The results support a model in which CO is adsorbed on metallic Au or at the Au/MO_x perimeter interface and reacts with oxygen also present at the Au/MO_x perimeter interface. The addition of MO_x to Au/Al_2O_3 (M = Cr, Mn, Fe, Co, Ni, Cu, and Zn) stabilized small Au particles. The observed activities were directly related to the average Au particle size, whereas the identity of MO_x is less important. The CH_4 oxidation activity of Au/Al_2O_3 is improved upon addition of MnO_x, FeO_x, CoO_x. The results presented pointed to the importance of Au/MO_x perimeter, which was defined as the boundary between Au, MO_x and the gas phase. The WGS reaction took place also at the perimeter interface of small gold particles and reduced cerium oxide surface. The importance of perimeter was also supported by DFT calculation on Au/TiO_2 system showing that the gas/metal/metal-oxide three-phase boundary systems greatly enhanced reactivity in the CO oxidation [38], and it was valid for an inverse titania/Au model catalyst [39].

Now we are in the position to tell something about the effect of preparation on the perimeter. In case of an active oxide supported gold system the interface between gold and oxide is primarily controlled by the particle size of the two components. However, if an inert oxide is applied as a support of the active oxide and gold there is a competition between the formation of active interfaces (Au with active oxide) and inactive interfaces (Au or active oxide with inert support). The stronger attraction between active oxide or its precursors (see e.g. TALH, Ti-propoxide or $Ce(NO_3)_3$) and Au particles stabilized by PDDA, or PVA favours the formation of more active system. The attraction is different depending on the sequence of deposition (oxide on Au/SBA-15 or Au on Ti/SBA-15) and this is why the particle size here becomes of secondary importance.

The effect of perimeter also depends on the size and morphology of the active oxide depending on whether it is used as promoter, when smaller oxide particles with modified crystal structures can be stabilised or as a well crystallized oxide support. In the case of ceria Lambert and co-workers [40] studied CO oxidation under UHV condition and found that it was strongly promoted on Pt(1 1 1) partially covered by ceria. CeO_2 overlayer was a much better catalyst when it was disordered compared with when it was ordered.

In the case of ceria the role of mobile oxygen cannot be excluded, either. Duprez [41] has shown, using isotope exchange reactions, that oxygen species are very mobile on ceria while they are not on silica. The oxygen mobility can be affected by the oxide structure, morphology, particle size, intimate contact with the support. The presence of non-metallic Au species can be also a factor to achieve higher activity of gold catalysts. Nanostructured gold supported on CeO_2 and SiO_2 were prepared by the deposition–precipitation and the solvated metal atom dispersion (SMAD) techniques [42]. The authors found that gold nanoparticles in a pure metallic state exhibited a worse catalytic performance, both on ceria and silica. However, in our samples prepared by the deposition of Au colloids reduced by borohydride the presence of non-metallic gold is hardly possible.

Nevertheless, the discrepancy observed in Figs. 9 and 10 is difficult to explain. It is believed that, similarly to Lambert's explanation [40], if ceria is amorphous the activity is significantly higher than when it is deposited on pure CeO_2. On the other hand, as we pointed out the active perimeter in the promoted SBA-15 supported samples cannot be determined. It is possible, that in TiO_2 promoted systems we could produce shorter active perimeter, than in the CeO_2 promoted one. Besides the morphological effect the possible contribution of different electron interactions in the systems cannot be ruled out, as well.

To sum up, the catalytic activity of inert oxide supported Au-active oxide system in the CO oxidation is primarily controlled by the anchoring properties between the active oxides and the gold nanoparticles if the particle sizes are similar. This dictates the length of active perimeter along the gold particles. In the case of ceria, in addition to the perimeter effect, the significantly higher activity is ascribed to the mobile oxygen which is more available in the not well crystallized ceria interfacing with gold, accelerating the reaction between CO and oxygen to form CO_2.

4. Conclusions

Au, Au-TiO_2 and Au-CeO_2 nanostructures were formed on different ways in SBA-15 support and were compared with the Au/SiO_2 and Au/TiO_2 and Au/CeO_2 analogous. The activity order in CO oxidation was *AuTiO$_2$_PVA* > *AuSBA_PVA_Ce* > *AuCeO$_2$_PVA* > *AuTiSBA_DP* > *AuTiSBA_PVA* > *AuSBA_PVA_Ti* ≈ *AuSBA_PVA* > *AuTiSiO$_2$_DP* > *AuTiSBA_PDDA* > *AuSBA_PDDA*.

It was shown that the activity is strongly affected not only by the Au particle size, but by the length of Au/TiO_2 or Au/CeO_2 perimeter, that is in good correlation with the surface charges of the components in the different preparations.

In SBA-15 the Au particles are more stable than in the SiO_2 supported sample resulting in increased activity (as compared *AuTiSBA_DP* and *AuTiSiO$_2$_DP*).

In Au/TiO_2/SBA system none of the preparation applied could produce large Au/TiO_2 interface, their catalytic activity is lower than that of *AuTiO$_2$_PVA*, the analogue Au/TiO_2 system.

Activity of *AuSBA_PVA_Ce* is significantly larger than that of the corresponding crystalline CeO_2 supported Au, *AuCeO$_2$_PVA*. This suggests that the Au/nanosize CeO_2 perimeter is more active than the Au/crystalline CeO_2 interface.

Acknowledgements

The authors are thankful to Mónika Urbán (University of Szeged) for preparation of SBA-15, György Sáfrán (Research Institute for Technical Physics and Materials Science, HAS) for HRTEM and Jenő Gubicza (Eötvös Loránd University) for XRD measurements. We acknowledge the financial help of the National Science and Research Fund (OTKA) grant #T-049564, #F-62481 and National Research and Development Program (NKFP 058/2004). The research was also supported by the COST D15/016/2001 and partly COST D36/003/2006 programs.

References

[1] M. Okumura, S. Nakamura, S. Tsubota, T. Nakamura, M. Azuma, M. Haruta, Catal. Lett. 51 (1998) 53.
[2] M.M. Schubert, S. Hackenberg, A.C. van Veen, M. Muhler, V. Plzak, R.J. Behm, J. Catal. 197 (2001) 113.
[3] D. Horváth, L. Tóth, L. Guczi, Catal. Lett. 67 (2000) 117.
[4] L. Guczi, G. Pető, A. Beck, K. Frey, O. Geszti, G. Molnár, Cs. Daróczi, J. Am. Chem. Soc. 125 (2003) 4332.
[5] L. Guczi, D. Horváth, Z. Pászti, L. Tóth, Z.E. Horváth, A. Karacs, G. Pető, J. Phys. Chem. B 104 (2000) 3183.
[6] H. Zhu, Z. Ma, J.C. Clark, Z. Pan, S.H. Overbury, S. Dai, Appl. Catal. A 326 (2007) 89.
[7] H. Zhu, C. Liang, W. Yan, S.H. Overbury, S. Dai, J. Phys. Chem. B 110 (2006) 10842.
[8] H. Zhu, Z. Ma, S.H. Overbury, S. Dai, Catal. Lett. 116 (2007) 128.
[9] J. Zhu, Z. Kónya, V.F. Puntes, I. Kiricsi, C.X. Miao, J.W. Ager, A.P. Alivisatos, G.A. Somorjai, Langmuir 19 (2003) 4396.
[10] Z. Kónya, E. Molnar, G. Tasi, K. Niesz, G.A. Somorjai, I. Kiricsi, Catal. Lett. 113 (2007) 19.
[11] C.-M. Yang, P.-H. Liu, Y.-F. Ho, C.-Y. Chiu, K.-J. Chao, Chem. Mater. 15 (2003) 275.
[12] C.-M. Yang, H.-A. Lin, B. Zibrowius, B. Spliethoff, F. Schüth, S.-C. Liou, M.-W. Chu, C.-H. Chen, Chem. Mater. 19 (2007) 3205.
[13] C.-W. Chiang, A. Wang, B.-Z. Wan, C.-Y. Mou, J. Phys. Chem. B 109 (2005) 18042.
[14] C.-W. Chiang, A. Wang, C.-Y. Mou, Catal. Today 117 (2006) 220.
[15] E. Sacaliuc, A.M. Beale, B.M. Weckhuysen, T.A. Nijhuis, J. Catal. 248 (2007) 235.
[16] W. Yan, V. Petkov, S.M. Mahurin, S.H. Overbury, S. Dai, Catal. Commun. 6 (2005) 404.
[17] W. Yan, S.M. Mahurin, B. Chen, S.H. Overbury, S. Dai, J. Phys. Chem. B 109 (2005) 15489.
[18] S. Mahurin, L. Bao, W. Yan, C. Liang, S. Dai, J. Non-Cryst. Solids 352 (2006) 3280.
[19] Z. Ma, S.H. Overbury, S. Dai, J. Mol. Catal. A: Chem. 273 (2007) 186.
[20] W. Yan, B. Chen, S.M. Mahurin, E.W. Hagaman, S. Dai, S.H. Overbury, J. Phys. Chem. B 108 (2004) 2793.
[21] M. Ruszel, B. Grzybowska, M. Laniecky, M. Wojtowski, Catal. Commun. 8 (2007) 1284.
[22] X. Xu, J. Li, Z. Hao, W. Zhao, C. Hu, Mater. Res. Bull. 41 (2006) 406.
[23] A.M. Venezia, F.L. Liotta, G. Pantaleo, A. Beck, A. Horváth, O. Geszti, A. Kocsonya, L. Guczi, Appl. Catal. A 310 (2006) 114.
[24] A. Horváth, A. Beck, A. Sárkány, Gy. Stefler, Zs. Varga, O. Geszti, L. Tóth, L. Guczi, J. Phys. Chem. B 110 (2006) 15417.
[25] L. Guczi, A. Beck, A. Horváth, A. Sárkány, Gy. Stefler, O. Geszti, Stud. Surf. Sci. Catal. 172 (2007) 221.
[26] F. Schüth, M. Comotti, B. Spliethoff, J. Am. Chem. Soc. 128 (2006) 917.
[27] T. Ungár, G. Tichy, J. Gubicza, R.J. Hellmig, Powder Diffraction 20 (2005) 366.
[28] J. Gubicza, T. Ungár, Z. Kristallogr. 222 (2007) 567.
[29] K.-W. Jun, H.-S. Roh, K.V.R. Chary, Catal. Surveys Asia 11 (2007) 97.
[30] R. Wang, H. Xu, Y. Chen, W. Li, Chin. J. Catal. 28 (2007) 293.
[31] F. Boccuzzi, A. Chiorino, S. Tsubota, M. Haruta, Sens. Actuators, B: Chem. B25 (1995) 540.
[32] H. Sakurai, M. Haruta, Catal. Today 29 (1996) 361.
[33] T. Hayashi, K. Tanaka, M. Haruta, J. Catal. 178 (1998) 566.
[34] M. Haruta, Stud. Surf. Sci. Catal. 145 (2002) 31.
[35] R.J.H. Grisel, C.J. Weststrate, A. Goossens, M.W.J. Crajé, A.M. Van der Kraan, B.A. Nieuwenhuys, Catal. Today 72 (2002) 123.
[36] R.J.H. Grisel, B.E. Nieuwenhuys, Catal. Today 64 (2001) 69.
[37] H. Sakurai, T. Akita, S. Tsubota, M. Kiuchi, M. Haruta, Appl. Catal. A: Gen. 291 (2005) 179.
[38] B. Hammer, L.M. Molina, W.X. Li, ACS National Meeting, Book of Abstracts, vol. 229, 2005, pp. PHYS-203.
[39] T.T. Magkoev, Surf. Sci. 601 (2007) 3143.
[40] C. Hardacre, R.M. Ormerod, R.M. Lambert, J. Phys. Chem. 98 (1994) 10901.
[41] D. Duprez, Stud. Surf. Sci. Catal. 112 (1997) 13.
[42] M.P. Casaletto, A. Longo, A.M. Venezia, A. Martorana, A. Prestianni, Appl. Catal. A 302 (2006) 309.